



Cite this: DOI: 10.1039/d0nr02276d



Received 21st March 2020

Accepted 8th June 2020

DOI: 10.1039/d0nr02276d

rsc.li/nanoscale

An active carbon-nanotube polarizer-embedded electrode and liquid-crystal alignment†

Tae Hyung Kim,^{‡a} Jong Gil Park,^{‡b,c} Yul Ki Kim,^d Young Jin Lim,^d Jae-Wook Kang,^{†a} Eun Sung Kim,^e Jeong Yong Kwon,^e Young Hee Lee ^{*b,c} and Seung Hee Lee ^{*d}

We report a method for constructing an active optical polarizer using an aligned carbon nanotube (CNT) sheet that is flexible, bendable, transparent, conductive, and also serves to anchor liquid-crystal (LC) molecules. A horizontally aligned CNT sheet was obtained by mechanical stretching from a vertically grown CNT forest, which was then transferred onto a substrate. A liquid polymer was infiltrated into the CNT sheet followed by UV curing, while a part of the CNT sheet was still exposed on the film surface without polymer coating. The polymer-embedded CNT sheet (P-ECS) film with 10 layers of CNT sheets exhibited a good polarization efficiency of 87%, a sheet resistance of $340 \Omega \square^{-1}$, and excellent ability to align LC molecules. The high stability of the P-ECS film was confirmed from the very low variation of sheet resistance (2%) and transmittance (10%) observed during a bending test of 1000 cycles. In addition, a twisted nematic LC device constructed using the P-ECS films shows a good bright–dark switching performance. The P-ECS film functions simultaneously as a transparent electrode, a film-type polarizer, and a LC alignment layer, demonstrating the multi-functionality of the active CNT film. This study thus highlights a wide range of possible applications for active polarizers and flexible displays.

Introduction

Carbon nanotubes (CNTs) could be viable alternatives to conventional materials used in electric devices owing to their

mechanical resilience,¹ high electrical conductivity,² optical transparency,^{2,3} high aspect ratio,⁴ and the possibility to anchor liquid crystal (LC) molecules on their surface.^{5,6} In particular, the aligned CNT array along a preferred direction leads to anisotropic optical absorption, therefore it has been intensively investigated for its applications in optical polarizers.^{7,8} There are three ways to align CNTs: (i) Aligned CNTs can be directly synthesized by chemical vapor deposition (CVD) on quartz substrates,⁹ (ii) fabric CNTs can be woven from a CNT forest,^{3,10} and (iii) using an external shear force¹¹ or electric/magnetic field to re-orientate CNTs dispersed in a liquid.^{12,13} However, the thickness and density of the aligned CNTs are limited in the direct synthesis method,¹⁴ and the degree of alignment from the reoriented CNTs in a liquid is very poor to meet the requirement of an optical polarizer.¹⁵ The aligned CNT sheets extracted from the CVD-grown CNT forest can function as flexible and active optical polarizers to offer comparable polarizer efficiency and the robust processing technique is suitable for industrial applications due to its scalability.³ However, the highly ordered CNT array is mechanically weak under external stresses such as bending, pressing, and strain. Therefore, the polymer-embedded CNT array has been intensively investigated to overcome this issue.^{16,17} The polymer effectively prevents the degradation of the aligned CNT array from the external stress. However, the CNT array is fully embedded within the polymer, limiting sheet conductance and more seriously prohibiting the LC anchoring effect on the CNT surface. In order to provide mechanical stability while retaining the inherent multi-functionality of the aligned CNT array, an exposure of CNTs on the polymer surface is a prerequisite condition for flexible LC display devices.^{18,19}

Herein, we report a method to fabricate a multi-functional optical polarizer using an aligned CNT sheet. The aligned CNT sheet was extracted by mechanically stretching it from a CNT forest and transferred onto a glass substrate, followed by polymer coating and UV curing with the partial exposure of CNTs. We were able to achieve high polarization efficiency, high conductance, and good LC alignment performance for

^aGraduate School of Flexible & Printable Electronics, Jeonbuk National University, Jeonju 54896, South Korea

^bCenter for Integrated Nanostructure Physics (CINAP), Institute for Basic Science (IBS), Sungkyunkwan University, Suwon 16419, Korea. E-mail: leeyoung@skku.edu

^cDepartment of Energy Science, Sungkyunkwan University, Suwon 16419, South Korea

^dDepartment of Polymer-Nano Science and Technology, Department of BIN Convergence Technology, Jeonbuk National University, Jeonju 54896, South Korea. E-mail: lsh1@jnbnu.ac.kr

^eR&D Center, A-Tech System Co., Incheon 21312, South Korea

†Electronic supplementary information (ESI) available. See DOI: 10.1039/d0nr02276d

‡These authors contributed equally to this work.

the polymer-embedded CNT sheet (P-ECS) film. The film showed excellent stability during a bending test of 1000 cycles. Compared to previous single-^{7,16} or dual-functional CNT array films such as a LC aligner-electrode system,^{18,19} we further demonstrated an active LC device using the multi-functional P-ECS film, which simultaneously acted as a transparent film-type polarizer, an electrode, and a LC alignment layer.

Results and discussion

The free-standing CNT sheet was extracted from a vertically grown multiwalled CNT (MWCNT) forest. One edge of the CNT forest was pulled mechanically in the form of a sheet and attached to a U-shaped guide (Fig. 1a). Free-standing CNT sheets were rotated using a mechanical motor for an increase in the number of CNT layers (n). The CNT sheets were then transferred onto the glass substrate (Fig. 1b). The transferred CNTs were preferentially aligned along the pulling direction, although slight deviations were present, as seen in the field-emission-scanning electron microscopy (FE-SEM) image (Fig. 1b). The polarization-angle dependent Raman spectra show a high degree of alignment of CNTs (inset of Fig. 1b and Fig. S1a in the ESI†). When the angle between the aligned axis of CNTs and the polarized axis of input light approaches from 0° to 90°, the normalized G-band (near 1575 cm⁻¹) intensity decreases due to the anisotropic absorption feature of CNTs.^{20,21} This also indicates the high degree of alignment of CNTs.

The liquid polymer (Norland Optical Adhesive 63, NOA63), which is an appropriate candidate matrix due to high transmittance (Fig. S1b, ESI†), was allowed to permeate into the CNT

sheets. The orientation ordering of CNTs in the P-ECS film was largely retained after UV curing. The CNTs were partially exposed at the bottom surface of the P-ECS film because of their direct, intimate contact with the glass substrate (Fig. 1c). This exposure of CNTs on the surface is the key to realizing an active CNT electrode with LC alignment. Only a few CNTs were partially exposed on the film surface, and hence the G-band Raman signal was negligible (Fig. S1c, ESI†). The polarization-angle dependent transmittance was measured to evaluate the degree of alignment of CNTs after polymer coating (Fig. S1d and e, ESI†). The transmittance (wavelength, $\lambda = 550$ nm, $n = 10$) both before (black symbols) and after polymer coating (red symbols) is reduced with an increased misorientation angle (θ , a polarized axis of the light from the aligned axis of CNTs). Although the transmittance was slightly decreased after polymer coating from 7.7% to 7.3% ($\lambda = 550$ nm, $\theta = 0^\circ$), no appreciable change was found (inset of Fig. 1c). By tilting the crossed polarizer-analyzer from 0° to 90°, the normalized brightness of the P-ECS film before and after the coating showed similar tendencies (Fig. S2, ESI†), which was confirmed by polarized optical microscopy (POM) measurements. The thickness of the CNT sheet was 3.6 μm with 8 CNT layers (Fig. S3, ESI†). As seen in the atomic force microscopy (AFM) images (Fig. 1e–g), the surface of the P-ECS film was grooved with a typical valley of 30–70 nm and a width of 2–3 μm , and the fine wrinkles were generated on the grooved surface by the individually exposed CNTs, irrespective of the number of CNT layers (Fig. S4, ESI†).

We measured the transmittance at $\lambda = 550$ nm ($T\%$ @550 nm) and sheet resistance (R_s) of the P-ECS films with a different number of CNT layers (Fig. 2a). Both $T\%$ @550 nm (Fig. S5, ESI†) and R_s decrease as the number of CNT layers increases. The transmittance reaches $\sim 42\%$ for 3 CNT layers, and R_s is as low as 340 $\Omega \square^{-1}$ for the sample with 10 layers. The variation in transmittance during the 1000 bending test is found to be very low ($\pm 10\%$) regardless of the number of layers in the range of 3–10 layers (Fig. 2b). The R_s value changes within $\pm 2\%$ (Fig. 2c). Since the R_s value is relatively high compared to those of previous studies (70–200 $\Omega \square^{-1}$),²² the R_s value can be further reduced by replacing MWCNTs with extremely high-conductive single-walled CNTs.

In the following, we describe the procedure to align LC molecules on the CNT surface. Due to π - π stacking, the

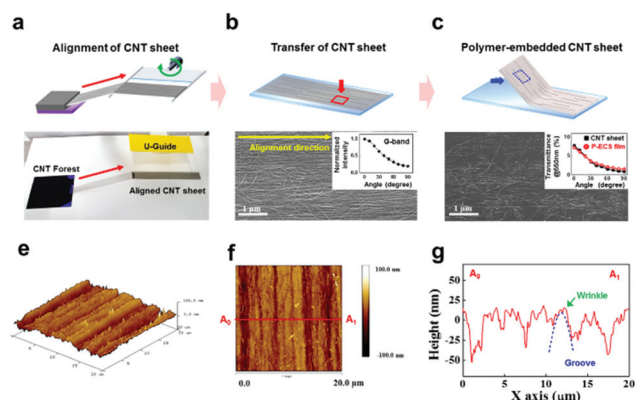


Fig. 1 Fabrication of a polymer-embedded CNT sheet (P-ECS) film. (a) Mechanical pulling for the alignment of CNTs, (b) a free-standing CNT sheet transferred on a substrate along with SEM image with the inset for polarization angle-dependent G-band (1575 cm⁻¹) intensity measured using a Raman microscope, and (c) polymer-coating: the SEM image of the back side showing CNTs without the polymer with the inset showing the polarization angle-dependent transmittance of the CNT sheet and P-ECS film at a wavelength of 550 nm. (d) AFM image of the surface of the P-ECS film: (e) 3D image, (f) 2D height morphology, and (g) line profile corresponding to the red line in (f).

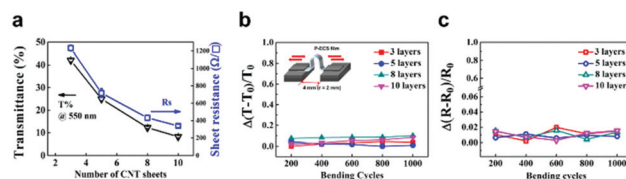


Fig. 2 (a) Transmittance at a wavelength of 550 nm and sheet resistance of the P-ECS film with a different number of CNT layers. The stability test showing relative changes in (b) transmittance and (c) sheet resistance during bending tests. The inset image in (b) is the schematic illustration of the bending tester.

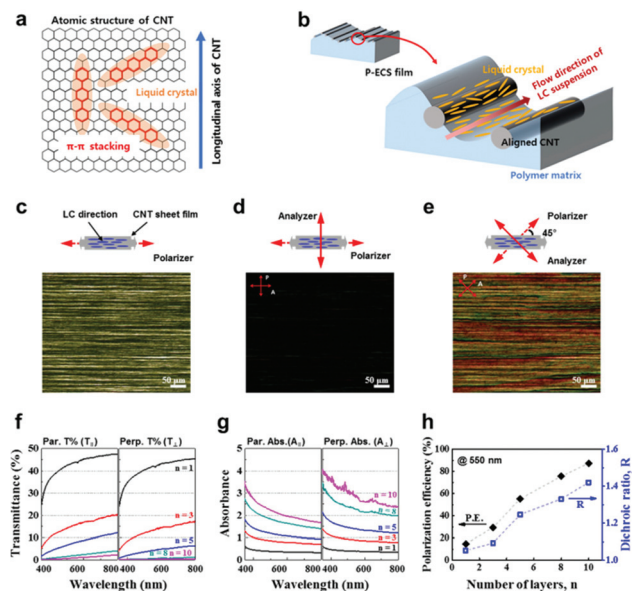


Fig. 3 Alignment of liquid crystals (LCs) on the surface of a P-ECS film: (a) π - π stacking between aromatic hexagonal rings in LC molecules (orange ellipsoid) and the hexagonal C-C network of the CNT. (b) Horizontally aligned LC molecules along the long axis of CNTs. Polarized optical microscopy measurement to evaluate LC alignment: LC-coated P-ECS film with (c) one polarizer (parallel direction, bright state), (d) crossed polarizer-analyzer (dark state), and (e) 45° tilted polarizer-analyzer (medium bright state). UV-Vis transmittance and absorbance spectra of two overlapped P-ECS films with various numbers of CNT layers: parallel and perpendicular (f) transmittance and (g) absorbance, and (h) polarization efficiency and dichroic ratio at 550 nm; n is the number of CNT layers.

anchoring of the aromatic hexagonal rings of the LC molecule on the CNT surface is energetically favored.^{5,6} In a typical LC molecule with 2–4 hexagonal rings, several orientations of the LC molecules are possible when anchored on the surface of CNTs (Fig. 3a). In neighboring LC molecules, they energetically prefer to align their long axes parallel to each other owing to steric hindrance. When the LC suspension is added dropwise onto the grooved P-ECS film, LC molecules flow along the groove direction and pile up on the aligned CNT surface. Consequently, at high LC density, the LC molecules are aligned preferentially along the long axis of the CNT surface (Fig. 3b).

The alignment of LC molecules was confirmed by POM for the LC-coated P-ECS film ($n = 8$). The incident light was linearly polarized using a polarizer located under the P-ECS film. The polarizer and the alignment direction of CNTs, as well as the LCs, are parallel to each other, resulting in a bright state (Fig. 3c). When the analyzer on top of the P-ECS film is oriented perpendicular to the polarizer, the linearly polarized light is blocked, resulting in a dark state (Fig. 3d). Upon rotation of the polarizer and analyzer by 45° with respect to the direction of alignment of CNTs, the birefringence of the LC molecules leads to retardation of the linearly polarized light, resulting in a medium bright state (Fig. 3e). Similar bright and dark states are observed for the sample with 5

layers (Fig. S6, ESI†). The pre-tilt angle of LC molecules was determined qualitatively by observing the luminance of the electrically controlled birefringence (ECB) device, which consists of two parallel P-ECS films with the injection of LC molecules. Using the symmetrical tiling ECB device ($\pm 10^\circ$, 20°), no significant change of luminance was observed (Fig. S7, ESI†). This concludes that the pre-tilt angle is close to 0° .

We measured the parallel ($T_{||}$) and perpendicular (T_{\perp}) transmittances of two overlapping P-ECS films with a different number of CNT layers (Fig. 3f, high magnification was provided in Fig. S8 a and b, ESI†). Both transmittances ($T_{||}$ and T_{\perp}) are reduced in the entire visible range as the number of CNT layers increases. At a given $\lambda = 550$ nm, the transmittance is reduced exponentially (Fig. S8c, ESI†). The parallel ($A_{||}$) and perpendicular (A_{\perp}) absorbance was calculated using $A = \log(1/T)$.²³ $A_{||}$ and A_{\perp} increase gradually as the number of CNT layers increases (Fig. 3g and Fig. S8d in the ESI†). The polarization performance can be evaluated from the polarization efficiency (PE), which is defined as,^{24,25}

$$PE = \sqrt{(T_{||} - T_{\perp}) / (T_{||} + T_{\perp})} \times 100 \quad (1)$$

Thus, PE is improved by increasing the number of CNT layers and it reaches 87% ($\lambda = 550$ nm, $n = 1$) (Fig. 3h) while remaining almost constant in the entire visible range (Fig. S8e, ESI†). The polarization performance can be evaluated by the degree of polarization (DOP) as well as the dichroic ratio. The DOP defined using $(T_{||} - T_{\perp}) / (T_{||} + T_{\perp})$ ²³ shows a similar dependence on the number of CNT layers to the PE result reaching ~ 0.72 at $\lambda = 550$ nm, $n = 10$ (Fig. S8f, ESI†). The dichroic ratio (R) is calculated by the ratio of parallel to perpendicular absorption coefficient ($A_{\text{par}}/A_{\text{perp}}$)^{24,26} The dichroic ratio ($\lambda = 550$ nm) increases gradually with an increasing number of CNT layers from 1.05 ($n = 1$) to 1.42 ($n = 10$) (Fig. 3h). These simply indicate that the polarization performance is improved with an increasing number of CNT layers, which is a trade-off to the transmittance.²⁴

Finally, we fabricated a twisted-nematic LC cell device using P-ECS films to simultaneously function as the electrode, polarizer, and LC alignment layer. LC molecules were placed in a gap with the help of spacer tape of 5 μm thickness, between two orthogonally stacked P-ECS films. Under these conditions, the molecules of the LC are twisted by 90° (left schematic of Fig. 4a). The light illuminated into the LC cell is transmitted through the cell *via* the twisted LC molecules, giving rise to a bright state (Fig. 4b). When voltage is applied between the top and bottom P-ECS films, the LC molecules are aligned vertically along the electric field owing to the positive dielectric anisotropy of the LC molecules. Here, P-ECS films act as an active medium. Thus, the LC cell ($n = 8$) shows the dark state at an applied voltage of 15 V (Fig. 4c).

The voltage-dependent transmittance (V - T) was measured for devices with a different number of CNT layers (Fig. 4d). The intensity was normalized using the relationship $(T\% - T\%_{\text{min}}) / (T\%_{\text{max}} - T\%_{\text{min}})$, where $T\%_{\text{min}}$ and $T\%_{\text{max}}$ are the minimum and maximum transmittance values in the V - T curve. The normal-

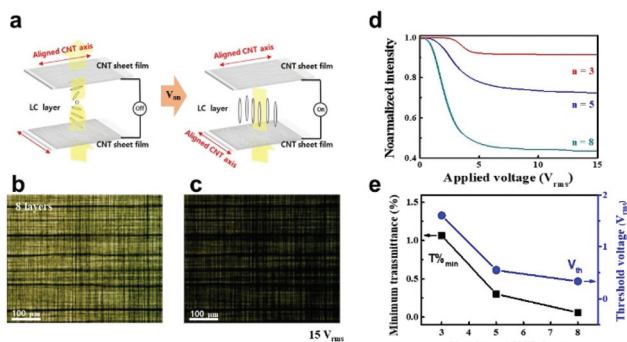


Fig. 4 Performance of the twisted-nematic LC cell device using P-ECS films: (a) Schematic illustration of an LC cell with and without applied voltage. Optical microscopy images of the LC cell device with 8 layers in (b) voltage-off and (c) -on states ($15 V_{rms}$). (d) Voltage-dependent normalized transmittance curves for devices with a different number of CNT sheets. (e) Threshold voltage (V_{th}) and the minimum transmittance ($T\%_{min}$) under an applied voltage of 15 V.

ized intensity decreases exponentially after an onset voltage of around 3 V and saturates around 10 V, irrespective of the number of CNT layers. The switching performance from the bright to dark state can be evaluated using the values of threshold voltage (V_{th}) defined as the voltage required to begin decreasing the normalized intensity. The V_{th} value slightly decreases with an increasing number of layers from 3 to 8 (blue symbols in Fig. 4e), which is mainly responsible for the improved electrical properties of the P-ECS film (Fig. 2a). To make a clear comparison of switch performance, we calculated V_{th} at 90% of normalized intensity ($V_{th\ 90\%}$).²⁷ (At $n = 3$, $V_{th\ 90\%}$ cannot be defined, since the normalized $T\%_{min}$ did not reach 90% due to the low polarization efficiency, PE ($n = 3$) = 29.4% at $\lambda = 550$ nm). The $V_{th\ 90\%}$ value also slightly decreases with an increasing number of layers from 5 to 8 (blue symbols in Fig. S9, ESI†). These $V_{th\ 90\%}$ values ($V_{th\ 90\%}$ ($n = 5$) = 1.7 V and $V_{th\ 90\%}$ ($n = 8$) = 1.3 V) are slightly lower than a simulated value of the standard cell ($V_{th\ 90\%} = 2.1$ V, Fig. S10 in the ESI†). Our switching performance is more sensitive than those reported in previous studies. The $V_{th\ 90\%}$ value of the LCD cell with the SiO₂-deposited CNT array was 4 V,²⁸ and the LCD cell with the randomly oriented CNT film as a transparent electrode varied with the $V_{th\ 90\%}$ value from 1.4 to 1.9 V.²⁷

This is ascribed to the relatively low polar anchoring energy ($W_{polar} = 6.43 \times 10^{-5}$ J m⁻²) of the P-ECS film cell compared to that ($\sim 10^{-4}$ J m⁻²) of the conventional polyimide alignment layer,²⁹ where W_{polar} was measured from capacitance–voltage (C – V) characteristics with elastic continuum theory.^{30,31} Detailed simulation of the standard cell and calculation of polar anchoring energy are explained in the ESI.†

The $T\%_{min}$ value of the LC cell after applying 15 V decreases for an increasing number of CNT layers (black symbols in Fig. 4e). The $T\%_{min}$ value at $n = 5$ decreases to 0.3%, resulting in light leakage even in the dark state (Fig. S11, ESI†). On the other hand, a reduction in $T\%_{min}$ to 0.06% is achieved for the device with $n = 8$, demonstrating a nearly ideal dark state

(Fig. 4c). Although we successfully obtained an active CNT polarizer film, the relatively poor alignment of CNTs in our device led to poor transmittance and polarizing properties when compared to those of the commercial polarizer (PE = 99%, $R = 25$). In addition, power consumption was relatively high in the LC cell device fabricated with the P-ECS film. Using single-walled CNTs instead of MWCNTs could be an option to improve the degree of alignment and to reduce power consumption.¹⁴ Furthermore, the high degree of alignment of CNTs could improve the transmittance, polarization performance and LC alignment, which could be realized by a more precise stretching process³² and transferring the directly grown horizontally aligned CNTs with high density.³³

Experimental section

Fabrication of the P-ECS film

One edge of a CNT forest (A-Tech System Co., Korea) was drawn as a sheet form using a U-shaped guide. The free-standing CNT sheet (15 mm × 70 mm) was transferred onto the hydrophobically treated glass substrate (25 mm × 70 mm). The CNT-transferred substrate was covered by another glass substrate (top) with spacer tape of 100 μm thickness. The UV-curable monomer (NOA 63, $n_p = 1.56$, Norland Products Inc.) was dropped at the gap entrance and then exposed to UV irradiation (Hamamatsu, LC8 L9588) of an intensity of 15 mW cm⁻² for 5 min. Finally, the P-ECS film was peeled off from the glass substrates.

Fabrication of the LC cell device (Fig. S12, ESI†)

The P-ECS film was supported by flat substrates (glass) to prevent bending. A metal wire was bound to the CNT-exposed face of the P-ECS film using silver paste. The LC molecular suspension (ZLI-4792, $\Delta n = 0.0969$, at 589 nm and 20 °C, $\Delta\epsilon = 5.3$, $T_{ni} = 92$ °C, Merck Advanced Technology) was added dropwise onto the film surface. Spacer tape of 5 μm-thickness was pasted on both the edge sides of the film along the longitudinal CNT direction. Another LC-coated P-ECS film was orthogonally laminated on the spacer (one drop filling method).

The degree of CNT alignment and the surface morphology were observed by FE-SEM (Hitachi SU-70) and AFM (Bruker, Multimode-8). The normal and polarized transmittances and Raman spectra were measured by UV-Vis spectroscopy (Scinco S-3100) in the 350–800 nm wavelength range and using a Raman microscope (NTEGRA Spectra, NT-MDT) with a wavelength of 532 nm, respectively. The sheet resistance was determined by non-contact eddy current probe measurements (Napson, EC-80P). The stability of the transmittance and the sheet resistance values of the P-ECS film were tested using an in-house bending test system. The bending radius was 2 mm, and the repeating step was 200 cycles. The alignment of LC molecules on the P-ECS film was confirmed by POM (Nikon, Eclipse E600 W POL). The voltage dependent-transmittance of the LC cell devices was measured using a LC measurement system (Sesim Photonics Technology, LCMS-200). The voltage-

dependent transmittance of the standard cell was simulated using a TechWiz LCD 2D tool (Sanayi System Co., Ltd). The polar anchoring energy was measured using a LCD physical properties measurement system (RDMS-200 and LCR meter, Agilent 4248A).

Conclusions

An active CNT polarizer film that is flexible, bendable, and transparent with good polarization efficiency was fabricated. The exposed CNTs rendered the surface conductive and brought about the alignment of LC molecules. Bending tests of 1000 cycles confirmed the excellent stability of transmittance and sheet resistance. Moreover, the bright–dark switching performance of the LC cell device using P-ECS films was reasonable. Our results thus demonstrate the multi-functional nature of the active CNT film and highlight its potential for diverse applications as flexible display, ultra-thin display, and so on. Furthermore, the multi-functional P-ECS film can lead to cost reduction by merging and replacing several components into one component.

Conflicts of interest

There are no conflicts to declare.

Acknowledgements

This research was supported by the Basic Science Research Program of the National Research Foundation of Korea (NRF) grant funded by the Ministry of Education (2016R1D1A1B01007189), the National Research Foundation of Korea (NRF) grant funded the Korea government (MSIT) (No. 2019R1A5A8080326), and the Institute for Basic Science of Korea (IBS-R011-D1).

Notes and references

- S. Pathak, J. R. Raney and C. Daraio, *Carbon*, 2013, **63**, 303–316.
- Z. Wu, Z. Chen, X. Du, J. M. Logan, J. Sippel, M. Nikolou, K. Kamaras, J. R. Reynolds, D. B. Tanner, A. F. Hebard and A. G. Rinzler, *Science*, 2004, **305**, 1273–1276.
- M. Zhang, S. Fang, A. A. Zakhidov, S. B. Lee, A. E. Aliev, C. D. Williams, K. R. Atkinson and R. H. Baughman, *Science*, 2005, **309**, 1215–1219.
- S. Iijima, *Nature*, 1991, **354**, 56–58.
- R. Basu and A. Garvey, *J. Appl. Phys.*, 2016, **120**, 164309.
- K. A. Park, S. M. Lee, S. H. Lee and Y. H. Lee, *J. Phys. Chem. C*, 2007, **111**, 1620–1624.
- L. Ren, C. L. Pint, L. G. Booshehri, W. D. Rice, X. Wang, D. J. Hilton, K. Takeya, I. Kawayama, M. Tonouchi, R. H. Hauge and J. Kono, *Nano Lett.*, 2009, **9**, 2610–2613.
- B. G. Kang, Y. J. Lim, K. U. Jeong, K. Lee, Y. H. Lee and S. H. Lee, *Nanotechnology*, 2010, **21**, 405202.
- C. Kocabas, S. H. Hur, A. Gaur, M. A. Meitl, M. Shim and J. A. Rogers, *Small*, 2005, **1**, 1110–1116.
- X. Zhang, K. Jiang, C. Feng, P. Liu, L. Zhang, J. Kong, T. Zhang, Q. Li and S. Fan, *Adv. Mater.*, 2006, **18**, 1505–1510.
- D. Wang, P. Song, C. Liu, W. Wu and S. Fan, *Nanotechnology*, 2008, **19**, 075609.
- T. Kimura, H. Ago, M. Tobita, S. Ohshima, M. Kyotani and M. Yumura, *Adv. Mater.*, 2002, **14**, 1380–1383.
- M. Monti, M. Natali, L. Torre and J. M. Kenny, *Carbon*, 2012, **50**, 2453–2464.
- R. Zhang, Y. Zhang and F. Wei, *Chem. Soc. Rev.*, 2017, **46**, 3661–3715.
- S. Wu, S. Peng and C. H. Wang, *Polymers*, 2018, **10**, 542.
- S. Shoji, H. Suzuki, R. P. Zaccaria, Z. Sekkat and S. Kawata, *Phys. Rev. B: Condens. Matter Mater. Phys.*, 2008, **77**, 153407.
- M. Jung, Y. Noh, D. Suh and S. E. Ahn, *Adv. Mater. Technol.*, 2018, **3**, 1800203.
- F. Roussel, J. F. Brun, A. Allart, L. M. Huang and S. O'Brien, *AIP Adv.*, 2012, **2**, 012110.
- T.-K. Truong, J. H. Park, M. D. A. Rahman, M. Urbanski, E. S. Kim, G. Scalia and D. Suh, *Curr. Appl. Phys.*, 2019, **19**, 162–167.
- G. S. Duesberg, I. Loa, M. Burghard, K. Syassen and S. Roth, *Phys. Rev. Lett.*, 2000, **85**, 5436–5439.
- J. G. Park, J.-G. Kim, K. P. So, J. Y. Hwang, E. S. Kim, J. Li, D. Suh and Y. H. Lee, *Carbon*, 2019, **153**, 513–524.
- Y. Zhou, R. Azumi and S. Shimada, *Nanoscale*, 2019, **11**, 3804–3813.
- M. Bass, *Handbook of optics Volume I Fundamentals, Techniques, and Design, 20.6 Optical density*, McGRAW-HILL, INC, 1995.
- E. Peeters, J. Lub, J. A. M. Steenbakkers and D. J. Broer, *Adv. Mater.*, 2006, **18**, 2412–2417.
- W. S. Lyoo, J. H. Yeum, J. M. Park, J. W. Kwak, J. H. Kim, S. S. Kim, B. C. Ji and S. K. Noh, *J. Appl. Polym. Sci.*, 2005, **96**, 967–974.
- H. Iwanaga, *Materials*, 2009, **2**, 1636–1661.
- W.-K. Lee, Y. S. Choi, Y.-G. Kang, J. Sung, D.-S. Seo and C. Park, *Adv. Funct. Mater.*, 2011, **21**, 3843–3850.
- W. Fu, L. Liu, K. Jiang, Q. Li and S. Fan, *Carbon*, 2010, **48**, 1876–1879.
- S. Hwang, H.-J. Jin, T.-H. Yoon and J. C. Kim, *Jpn. J. Appl. Phys.*, 2010, **49**, 121702.
- Y. Toko and T. Akahane, *Mol. Cryst. Liq. Cryst. Sci. Technol., Sect. A*, 2001, **368**, 469–481.
- Y. Liu, J. Sang, H. Liu, H. Xu, S. Zhao, J. Sun, J. H. Lee, H.-C. Jeong and D.-S. Seo, *Crystals*, 2019, **9**, 181.
- X. Wang, Z. Z. Yong, Q. W. Li, P. D. Bradford, W. Liu, D. S. Tucker, W. Cai, H. Wang, F. G. Yuan and Y. T. Zhu, *Mater. Res. Lett.*, 2012, **1**, 19–25.
- S. J. Kang, C. Kocabas, H. S. Kim, Q. Cao, M. A. Meitl, D. Y. Khang and J. A. Rogers, *Nano Lett.*, 2007, **7**, 3343–3348.